Scaling of ion trapping in laser-driven relativistically transparent plasma

B. Liu,[1] J. Meyer-ter-Vehn,[2] and H. Ruhl[1]

[1]*Institute for Computational and Plasma Physics, Ludwig-Maximilian-Universitaet, Muenchen, 80333 Muenchen, Germany*

[2]*Max-Planck-Institut für Quantenoptik, D-85748 Garching, Germany*

Abstract

Ion trapping by ion wave breaking is investigated for laser-driven near-critical relativistically transparent plasma. Guided by three-dimensional particle-in-cell simulations, we study ion motion along the laser propagation direction within a 1D fluid model. The threshold for ion trapping is found, and the singular behaviour of longitudinal electric field, ion velocity, and ion density in the vicinity of the ion wave breaking point is derived analytically showing power-law distributions. The important result is that only a fraction of ions is trapped, different from the regime of hole boring. The number of trapped particles is determined and how it depends on target density for fixed laser intensity. Results are confirmed by the simulations.

Recent developments of ultra-intense laser technology have opened new options for laser-driven plasma-based ion acceleration [1]. Ions are trapped and accelerated in a localized charge-separation field, comoving with the propagating laser pulse. Relativistically transparent plasma [2] close to the critical density is of particular interest [3–7], because pulse propagation slows down and thus eases trapping of background ions. Simulations have shown superior characteristics such as high ion energy [3, 6, 7], narrow energy spread [3], and low beam emittance [7]. Moreover, it is possible to further improve the acceleration by shaping the plasma density. This may become feasible with new techniques of preparing targets in the near-critical density regime [8–12].

Here we address ion trapping by ion wave breaking, a mechanism that has not been studied in sufficient detail, so far. The general scenario is that the laser pulse ionizes the target material, pushes a high-density layer of relativistic electrons at the front, and leaves behind a region occupied only by ions [13]. Charge separation builds up a longitudinal electric field that drives an ion wave with phase velocity equal to the laser front velocity v_f. It turns out that the ion motion evolves along the laser axis and allows approximately for one-dimensional (1D) modelling. When driven strongly [14], the ion wave breaks, such that background ions are trapped and accelerated to velocities far above v_f. The interesting point is that this trapping process is self-regulating and stops when a fraction of ions is trapped. This can be controlled by external parameters such as laser intensity and target density. It allows to design ion pulses with low energy spread and beam emittance. It makes ion wave breaking acceleration different from the regime of hole boring [15], where all ions in the laser focus are accelerated and which applies to opaque plasma. In the following, we treat ion trapping by wave breaking analytically within a 1D fluid model. Results are then compared with 3D particle-in-cell (PIC) simulations.

For simplicity, we assume that the plasma is composed of electrons and only one kind of ions, having number densities n_e and n_i, respectively. The ion motion in the region of electron depletion ($n_e \approx 0$) is described by the equations

$$\frac{\partial n_i}{\partial t} + \frac{\partial}{\partial z}(n_i v_i) = 0, \tag{1}$$

$$\left(\frac{\partial}{\partial t} + v_i \frac{\partial}{\partial z}\right)(m_i \gamma_i v_i) = q_i E_z, \tag{2}$$

$$\frac{\partial}{\partial z} E_z = \frac{1}{\epsilon_0} q_i n_i, \tag{3}$$

where z denotes the laser propagation direction, v_i the ion velocity along the z-axis, $\gamma_i = 1/\sqrt{1-\beta_i^2}$, $\beta_i = v_i/c$, c the light speed in vacuum, q_i the ion charge, m_i the ion mass, E_z the longitudinal electric field, and ϵ_0 the vacuum permittivity.

In the frame comoving with the laser front, we look for stationary propagating solutions $n_i(\xi)$, $\beta_i(\xi)$, and $E_z(\xi)$, where the comoving coordinate is $\xi = \omega_i(z/v_f - t)$. Introducing also dimensionless quantities $\tilde{n}_i = q_i n_i/en_0$, and $\tilde{E} = E_z/E_0$, where $E_0 = m_i c\omega_i/q_i$, $\omega_i = \sqrt{q_i e n_0/m_i\epsilon_0}$ is the ion oscillation frequency, e denotes the electron charge, and n_0 the initial plasma density, Eqs. (1,2,3) transform into

$$\frac{d}{d\xi}(\tilde{n}_i - \tilde{n}_i\beta_i/\beta_f) = 0, \tag{4}$$

$$(1-\beta_i/\beta_f)\frac{d\gamma_i\beta_i}{d\xi} = -\tilde{E}, \tag{5}$$

$$\frac{d\tilde{E}}{d\xi} = \beta_f\tilde{n}_i, \tag{6}$$

where $\beta_f = v_f/c$. The ion density,

$$\tilde{n}_i = \frac{1}{1-\beta_i/\beta_f}, \tag{7}$$

is obtained directly from Eq. (4); it satisfies $\tilde{n}_i = 1$ ahead of the laser front, where ions are at rest ($\beta_i = 0$). Ions oscillate in the longitudinal electric field E_z. They first acquire velocity in laser direction ($\beta_i > 0$) in the upstream region, where $E_z > 0$, but then loose it again in the downstream region where $E_z < 0$. The interesting case, now to be studied in detail, occurs when the ion velocity reaches the velocity of the laser front ($\beta_i = \beta_f$) at the point where E_z switches sign (chosen here as $\xi = 0$). According to Eq. (7), the ion density diverges at this point, and the downstream ion flow is disrupted. Ions are then reflected back into the accelerating region ($\xi > 0$). Furthermore, combining Eqs. (5,6,7), we obtain

$$\frac{d}{d\xi}\left(\frac{\tilde{E}^2}{2} + \beta_f\gamma_i\beta_i\right) = 0. \tag{8}$$

Integrating this equation from $\xi = 0$, where $\beta_i = \beta_f$ and $\tilde{E} = 0$, we find for the maximum electric field occuring close to the laser front, where $\beta_i \ll \beta_f$,

$$\tilde{E}_{\mathrm{IWB}} = \beta_f\sqrt{2\gamma_f}; \tag{9}$$

here $\gamma_f = 1/\sqrt{1-\beta_f^2}$. This gives the field $E_{\mathrm{IWB}} = E_0\tilde{E}_{\mathrm{IWB}}$ required for ion wave breaking; we call it ion wave breaking field [16, 17]. It has to be provided by the laser pulse at the

laser front. In the case that the maximum field $E_{\max}$ driven by the laser pulse becomes larger than E_{IWB}, ion trapping sets in.

We now investigate the ion flow close to wave breaking conditions in more detail. We focus on local solutions of Eqs. (5,6,7) near the ion wave breaking point ($\xi \to 0$) and in the accelerating region ($\xi > 0$). We try the power-law ansatz

$$\tilde{n}_i(\xi) = \Lambda \xi^{\Theta}, \tag{10}$$

with $\Lambda > 0$ and $\Theta < 0$. Applying it to Eqs. (5,6,7) and making use of the identity $d(\beta\gamma) = \gamma^3 d\beta$, we find

$$\frac{\gamma_f^3 \beta_f \Theta}{\xi^{1+\Theta}\Lambda} = -\frac{\beta_f \xi^{1+2\Theta}\Lambda^2}{(1+\Theta)}. \tag{11}$$

Comparing exponents of ξ and front coefficients on both sides, we get

$$\Theta = -2/3, \quad \Lambda = 2^{1/3}\gamma_f/3^{2/3}. \tag{12}$$

Finally, we have

$$\tilde{E}(\xi) = 2^{1/3}\beta_f\gamma_f(3\xi)^{1/3}, \tag{13}$$

$$(1 - \beta_i(\xi)/\beta_f) = 2^{-1/3}(3\xi)^{2/3}/\gamma_f, \tag{14}$$

$$\tilde{n}_i(\xi) = 2^{1/3}\gamma_f/(3\xi)^{2/3}. \tag{15}$$

Apparently, the singular behaviour in the vicinity of the wave breaking point is characterised by a set of critical point exponents. This reflects the fact that wave breaking is a kind of critical phenomenon [18].

As soon as trapping sets in, a flow of reflected ions is superimposed to the flow of incoming ions in the region $\xi > 0$ close to the wave breaking point. Shortly after reflection, the bunch of trapped ions moves almost with the laser front velocity and can also be described approximately by quasi-stationary distributions of density $n_{ir}(\xi)$ and velocity $\beta_{ir}(\xi)$, satisfying

$$\frac{d}{d\xi}(\tilde{n}_{ir} - \tilde{n}_{ir}\beta_{ir}/\beta_f) = 0, \tag{16}$$

$$(1 - \beta_{ir}/\beta_f)\frac{d(\gamma_{ir}\beta_{ir})}{d\xi} = -\tilde{E}, \tag{17}$$

just as the incoming flow; here $\gamma_{ir} = 1/\sqrt{1-\beta_{ir}^2}$. We now denote density and velocity of the incoming flow by $\tilde{n}_{ii}$ and β_{ii}, respectively. The difference in this two fluid approach is

that Poisson's equation now includes the charge distribution of both flows:

$$\frac{d\tilde{E}}{d\xi} = \beta_f(\tilde{n}_{ii} + \tilde{n}_{ir}). \tag{18}$$

Since the downstream ion flow is disrupted, when wave breaking sets in, we have the boundary condition $\tilde{n}_{ii}(1-\beta_{ii}/\beta_f) + \tilde{n}_{ir}(1-\beta_{ir}/\beta_f) = 0$ at $\xi = 0$ and since also densities match for $\xi \to 0$, again the ansatz $\tilde{n}_{ii} = \tilde{n}_{ir} = \Lambda\xi^{\Theta}$ can be made near $\xi = 0$ for both the incoming and the reflected ions. By using the same approach as before in deriving Eqs. (13,14,15), we find the power-law distributions

$$\tilde{E}(\xi) \;=\; 2\beta_f\gamma_f(3\xi)^{1/3}, \tag{19}$$

$$(\beta_{ir}(\xi)/\beta_f - 1) = (1-\beta_{ii}(\xi)/\beta_f) \;=\; (3\xi)^{2/3}/\gamma_f, \tag{20}$$

$$\tilde{n}_{ir}(\xi) = \tilde{n}_{ii}(\xi) \;=\; \gamma_f/(3\xi)^{2/3}, \tag{21}$$

for the combined flow of incoming and reflected ions. The total ion density becomes

$$\tilde{n}_i(\xi) = \tilde{n}_{ii}(\xi) + \tilde{n}_{ir}(\xi) = 2\gamma_f/(3\xi)^{2/3}. \tag{22}$$

One observes that the power-law exponents are the same as before, but the amplitudes have changed. Both the electric field and the total ion density have increased by a factor $2^{2/3}$, when compared with Eqs. (13,15).

The increase in electric field eventually closes the gap between the maximum field $E_{\max}$ driven by the laser pulse and intrinsic wave breaking field, and then trapping stops. At this time, the trapped ions have expanded over a short distance $\Delta\xi$, and their areal density is

$$\tilde{\mathcal{N}}_{ir} = \int_0^{\Delta\xi} \tilde{n}_{ir}(\xi)d\xi = (3\Delta\xi)^{1/3}\gamma_f. \tag{23}$$

The analogue to Eq. (8) now reads

$$\frac{d}{d\xi}\left(\frac{\tilde{E}^2}{2} + \beta_f\gamma_{ii}\beta_{ii}\right) = \beta_f\tilde{E}\tilde{n}_{ir}. \tag{24}$$

Integrating again from $\xi = 0$ to the laser front and making use of Eqs. (9,19,21), we get

$$(\tilde{E}^2_{\max} - \tilde{E}^2_{\rm IWB})/2 = \beta_f^2\gamma_f^2(3\Delta\xi)^{2/3}. \tag{25}$$

It allows us to eliminate $\Delta\xi$ in Eq. (23) and to calculate the trapped charge per area. In dimensional units with $\mathcal{N}_{\rm trap} = (n_0 v_f/\omega_i)\tilde{\mathcal{N}}_{ir}$, we get

$$q_i\mathcal{N}_{\rm trap} = \frac{q_i}{e}\epsilon_0 E_{\rm IWB}\left(\frac{1}{2}\left(E^2_{\max}/E^2_{\rm IWB} - 1\right)\right)^{1/2}. \tag{26}$$

This is the central result of the present work. It gives the trapped charge per area in terms of the displacement $\epsilon_0 E_{\rm IWB}$, corresponding to the threshold electric field for ion wave breaking, and a factor describing the onset of trapping for $E_{\rm max} > E_{\rm IWB}$.

Both $E_{\rm max}$ and $E_{\rm IWB}$ depend on laser amplitude a_0 and plasma density n_0. For fixed a_0, the threshold for ion wave breaking is defined by $E_{\rm max}(n_0^*) = E_{\rm IWB}(n_0^*)$ and allows to calculate the threshold density n_0^*. Here, we mark all quantities taken at the wave breaking threshold by an asterisk. Introducing $F(n_0) = E_{\rm max}^2/E_{\rm IWB}^2$, such that $F(n_0^*) = 1$, and expanding $F(n_0)$ around $n_0 = n_0^*$, we get $F(n_0) = 1 + f_0(n_0/n_0^* - 1)$, where $f_0 = n_0^* \partial F(n_0^*)/\partial n_0^*$. We then find the trapped charge per area in the form

$$q_i \mathcal{N}_{\rm trap} \approx f_1 \frac{q_i}{e} \epsilon_0 E_0^* \left(\frac{n_0}{n_0^*} - 1 \right)^{1/2}, \tag{27}$$

with $f_1 = \beta_f^* (f_0 \gamma_f^*)^{1/2}$. This result holds for fixed laser intensity and densities n_0 close to threshold density n_0^*, a region distinguished by high final ion energy and low energy spread. The precise values of the front factors depend on details not treated in the present 1D model. Comparing with simulation results in the following, they turn out to be of order one. We emphasize that the important analytic result concerns the scaling exponent and that the square root dependence in Eq. (27) traces back to the exponents in Eqs. (19,21).

We have carried out 3D PIC simulations to verify the model predictions, using the plasma simulation code (PSC) [19]. A laser pulse with circular polarization and wavelength $\lambda_L = 1\mu$m is vertically incident on hydrogen plasma ($m_i/m_e = 1836$ and $q_i/e = 1$) with bulk density $n_0 = 7.2 n_c$; here $n_c = m_e \omega_L^2 \epsilon_0 / e^2$ denotes the critical plasma density, m_e the electron mass, and ω_L the laser frequency. At the surface, the density rises in the region $0 < z < z_n$ according to $n(z) = n_0 \exp(-(z - z_n)^2/\sigma_n^2)$ with $z_n = 3\mu$m and $\sigma_n = 0.63\mu$m. The laser intensity is $I_0 = 6 \times 10^{20}$W/cm^2, corresponding to laser amplitude $a_0 = 15$. We have chosen a relatively low value of intensity to demonstrate that ion trapping by ion wave breaking can already be studied with laser pulses presently available experimentally. Also, the shape of the pulse incident from the left side ($z = 0$) is modelled by a Gaussian amplitude $a(r,t) = a_0 \exp(-r^2/R_L^2) \exp(-(t - t0)^2/\tau_L^2)$ with pulse time $\tau_L = 33.33$ fs (10 laser cycles), focal radius $R_L = 3\mu$m, and $t_0 = 66.67$ fs, implying a moderate contrast ratio at the pulse front. In order to resolve details of ion motion, in particular near the wave breaking point, we have chosen 50 cells per micron and 10 macro-particles per cell for each species. The initial temperatures are set to 10 keV for electrons and 1 keV for ions.

Simulation results are displayed in Fig. 1 as snapshots at different times of on-axis distributions (radially averaged over $|r| < 0.2$ μm): ion and electron density are shown in the first row, longitudinal electric field in the second row, and ions phase space $(p_z/m_ic, z)$ in the third row. At 55 fs (first column), the ion wave develops a sharp peak in density at $z \approx 2.945$ μm and is about to break. The local distributions near the ion wave breaking point match well with the power-law scalings given by Eqs. (13,14,15) (dotted black lines). The laser front velocity is equal to ion velocity at the wave breaking point, and we find $\beta_f^* \approx p_z/m_ic \approx 0.1$ from Fig.1(c). Somewhat later at 60 fs (second column), ion wave breaking is in progress, and a good portion of the ions has already been reflected and is accelerating in the region $z > 3.1$ μm. Ion density and electric field have increased in agreement with the model results, now given by Eqs. (19,20,21). Later at 86 fs (third column), an ion bunch is observed at $z = 4.7\mu$m, both in parts (g) and (i) of the figure. The bunch propagates to the right with speed $\beta_i \approx 0.3$, about three times faster than β_f^*. It corresponds to a proton energy of (40 ± 10) MeV at this time, but it will further gain energy (reaching about 65 MeV), before overtaking the laser front and then freely cruising to the right. It is noticed that, different from the model prediction, ion trapping is not suppressed completely. Rather a thin tail of ions is attached to the main ion bunch, be it of much reduced ion energy density. This feature is attributed to the time dependence of the incident laser pulse and also to self-focusing which leads to an increase of laser intensity on axis during the acceleration period. This is not accounted for in the model. We find, however, that this has little influence on the number of trapped ions, which represents the central interest of the present work. Actually, the trapped charge per area almost stagnates shortly after wave breaking.

In Fig. 2 (a), we compare values of $\mathcal{N}_{\rm trap}$ from simulations with that from Eq. (27) for laser pulses having very different amplitudes: case 1 with $a_0 = 15$ (blue, same as in Fig. 1) and case 2 with $a_0 = 155$ (black, reported in Ref. [7]). They correspond to threshold densities $n_0^* = 6.5n_c$ for case 1 and $n_0^* = 1.8n_c$ for case 2. The simulations are well described by the square root scaling, represented by the straight lines with slope 1/2 in the double-logarithmic plot. The position of these lines has been adjusted by choosing in Eq. (27) $f_1 = 0.25$ for case 1 and $f_1 = 0.75$ for case 2. It demonstrates that the present scaling result holds over laser intensities ranging from 10^{20} to 10^{22}W/cm^2 and beyond. The 3D PIC simulations provide us with absolute numbers of accelerated ions; they are plotted in

Fig. 2 (b). In the simulations, they appear as bullet-like beam bunches with transverse dimensions Δr similar to the longitudinal one Δz, which is known from Eqs. (9) and (25) to be $\Delta z = (c\beta_f^*/\omega_i^*)\Delta\xi$ with $\Delta\xi \approx ((E_{\max}^2/E_{\rm IWB}^2 - 1)/\gamma_f^*)^{3/2}/3$. We may therefore estimate the absolute number of trapped and accelerated ions as

$$N_{\rm trap}^{\rm 3D} \approx (\Delta r)^2 \mathcal{N}_{\rm trap} \approx f_2 \left(\frac{c}{\omega_i^*}\right)^2 \frac{\epsilon_0 E_0^*}{e} \left(\frac{n_0}{n_0^*} - 1\right)^{7/2}. \tag{28}$$

The straight lines in Fig. 2 (b) with slope 7/2 appear to describe the behaviour of the simulation points quite well. Here we have used adjustment factors $f_2 = 2$ for case 1 and $f_2 = 0.4$ for case 2. For high laser amplitudes, $a_0 > 100$, bunches of 10^{11} protons and more are predicted.

In summary, we have identified the dynamics of self-regulating ion trapping in a laser-driven charge-separation field as a process of essentially one-dimensional ion wave breaking. We succeeded to determine the power-law profiles of ion flow at the instant of wave breaking and the finite amount of charge that is trapped and accelerated. The critical electric field for ion wave breaking, $E_{\rm IWB}$, has been found as a function of laser front velocity, and the trapped ion charge depends on how much the maximum field $E_{\max}$ driven by the laser pulse exceeds $E_{\rm IWB}$. This can be controlled by tuning laser intensity and plasma density. Near threshold, this charge is small and localized such that high-quality ion bunches with low energy spread and beam emittance are expected. We hope that the present results stimulate experiments to explore this regime; it occurs in relativistically transparent laser plasma, just below the regime of hole boring.

B. Liu acknowledges support from the Alexander von Humboldt Foundation. B. Liu and H. Ruhl acknowledge support by the Gauss Centre for Supercomputing (GCS) Large-Scale Project (Project Nos. pr92na, pr74si), the Cluster-of-Excellence Munich Centre for Advanced Photonics (MAP), and the Arnold Sommerfeld Center (ASC) at Ludwig-Maximilians University of Munich (LMU). B. Liu also thanks J. Schreiber for providing computing resources on the HYDRA supercomputer at Max-Planck-Institute für Quantenoptik (MPQ).

---

[1] H. Daido, M. Nishiuchi, and A. S. Pirozhkov, Rep Prog Phys **75**, 056401 (2012); A. Macchi, M. Borghesi, and M. Passoni, Rev. Mod. Phys. **85**, 751 (2013); M. Borghesi, Nucl. Instr. Meth.

A**740**, 6 (2014); J. Schreiber, P. R. Bolton, and K. Parodi, Rev. Sci. Instrum. **87**, 071101 (2016).

[2] P. Kaw, Phys. Fluids **13**, 472 (1970).

[3] A. P. L. Robinson, Physics of Plasmas **18**, 056701 (2011).

[4] S. M. Weng, M. Murakami, P. Mulser, and Z. M. Sheng, New J. Phys. **14**, 063026 (2012).

[5] A. A. Sahai, F. S. Tsung, A. R. Tableman, W. B. Mori, and T. C. Katsouleas, Phys. Rev. E **88**, 043105 (2013).

[6] A. V. Brantov, E. A. Govras, V. F. Kovalev, and V. Y. Bychenkov, Phys. Rev. Lett. **116**, 085004 (2016).

[7] B. Liu, J. Meyer-ter-Vehn, K.-U. Bamberg, W. J. Ma, J. Liu, X. T. He, X. Q. Yan, and H. Ruhl, Phys. Rev. Accel. Beams **19**, 073401 (2016).

[8] W. Ma, L. Song, R. Yang, T. Zhang, Y. Zhao, L. Sun, Y. Ren, D. Liu, L. Liu, J. Shen, Z. Zhang, Y. Xiang, W. Zhou, and S. Xie, Nano Lett. **7**, 2307 (2007).

[9] L. Willingale, S. R. Nagel, A. G. R. Thomas, C. Bellei, R. J. Clarke, A. E. Dangor, R. Heathcote, M. C. Kaluza, C. Kamperidis, S. Kneip, K. Krushelnick, N. Lopes, S. P. D. Mangles, W. Nazarov, P. M. Nilson, and Z. Najmudin, Phys. Rev. Lett. **102**, 125002 (2009).

[10] Y. Fukuda, A. Y. Faenov, M. Tampo, T. A. Pikuz, T. Nakamura, M. Kando, Y. Hayashi, A. Yogo, H. Sakaki, T. Kameshima, A. S. Pirozhkov, K. Ogura, M. Mori, T. Z. Esirkepov, J. Koga, A. S. Boldarev, V. A. Gasilov, A. I. Magunov, T. Yamauchi, R. Kodama, P. R. Bolton, Y. Kato, T. Tajima, H. Daido, and S. V. Bulanov, Phys. Rev. Lett. **103**, 165002 (2009).

[11] J. H. Bin, W. J. Ma, H. Y. Wang, M. J. V. Streeter, C. Kreuzer, D. Kiefer, M. Yeung, S. Cousens, P. S. Foster, B. Dromey, X. Q. Yan, R. Ramis, J. Meyer-ter-Vehn, M. Zepf, and J. Schreiber, Phys. Rev. Lett. **115**, 064801 (2015).

[12] A. V. Brantov, E. A. Obraztsova, A. L. Chuvilin, E. D. Obraztsova, and V. Y. Bychenkov, Phys. Rev. Accel. Beams **20**, 061301 (2017).

[13] T. Schlegel, N. Naumova, V. T. Tikhonchuk, C. Labaune, I. V. Sokolov, and G. Mourou, Physics of Plasmas **16**, 083103 (2009).

[14] Practically, this occurs at laser intensities above $10^{20}\mathrm{W/cm}^2$, now available.

[15] S. C. Wilks, W. L. Kruer, M. Tabak, and A. B. Langdon, Phys. Rev. Lett. **69**, 1383 (1992); A. Macchi, F. Cattani, T.V. Liseykina, and F. Cornolti, Phys. Rev. Lett. **94**, 165003 (2005).

[16] We note that this threshold result is essentially the same as that known for 1D electron wave

breaking [17] in the relativistic limit, except that the normalization field is a factor $\sqrt{q_i m_i / e m_e}$ larger.

[17] A. I. Akhiezer and R. V. Polovin, JETP Lett. 3, 696 (1956).

[18] See, e.g., H. E. Stanley, *Introduction to Phase Transitions and Critical Phenomena* (Oxford University Press, New York, 1971), Chap. 2.

[19] H. Ruhl, Classical particle simulations, in *Introduction to Computational Methods in Many Body Physics*, edited by M. Bonitz, and D. Semkat (Rinton, Paramus, New Jersey, 2006).

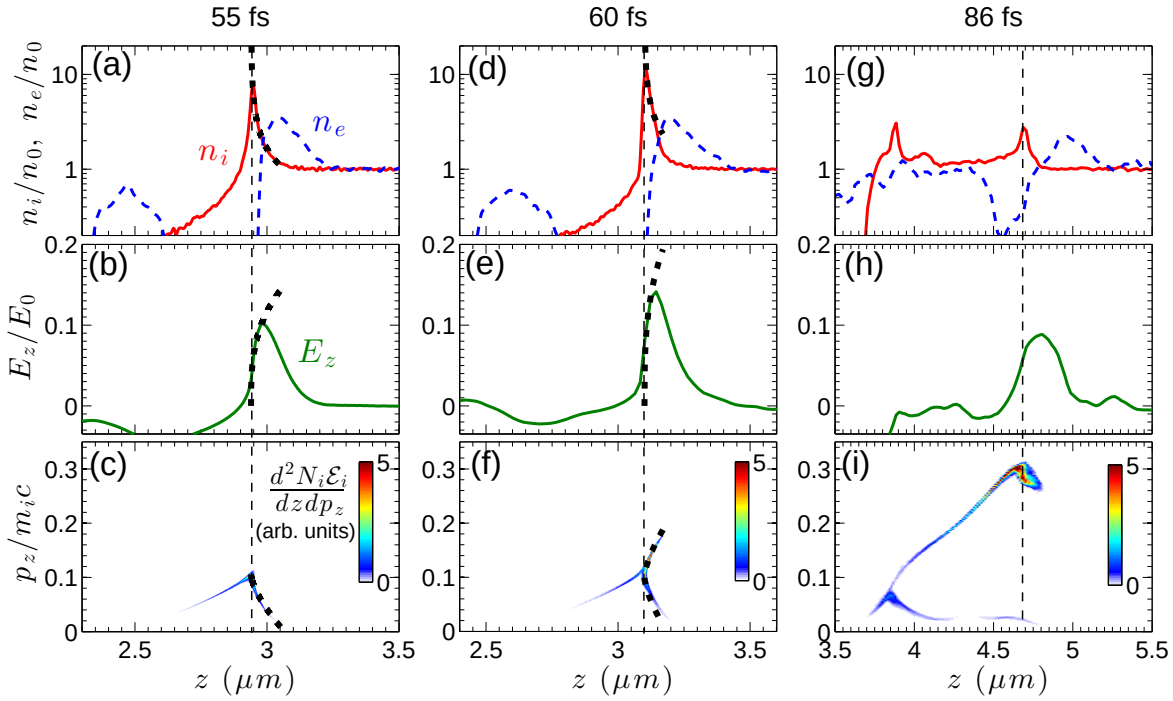

FIG. 1: Comparison of 3D PIC simulation with the 1D model (black dotted curves in the first two columns) near the point of ion wave breaking, showing (a,d,g) ion density n_i/n_0 (red solid line), electron density n_e/n_0 (blue dashed line), (b,e,h) longitudinal electric field E_z/E_0 (green solid line), and (c,f,i) ion kinetic energy density ($d^2N_i\mathcal{E}_i/dzdp_z$ in arbitrary units) in phase space $(z, p_z/m_ic)$ on the laser axis (averaged over $|r| < 0.2\mu$m). The first column (a,b,c) refers to the onset of ion wave breaking at 55 fs. The middle column (d,e,f) shows ion trapping at 60 fs. The dashed vertical lines mark the ion wave breaking points in the first two columns. Column (g,h,i) shows the results at 86 fs, when trapping stops and the ion bunch, marked by the dashed vertical line, is still accelerating. These results correspond to a laser intensity of $I_0 = 6 \times 10^{20}$W/cm^2 ($a_0 = 15$) and a hydrogen plasma density of $n_0 = 7.2 n_c$; for details see text.

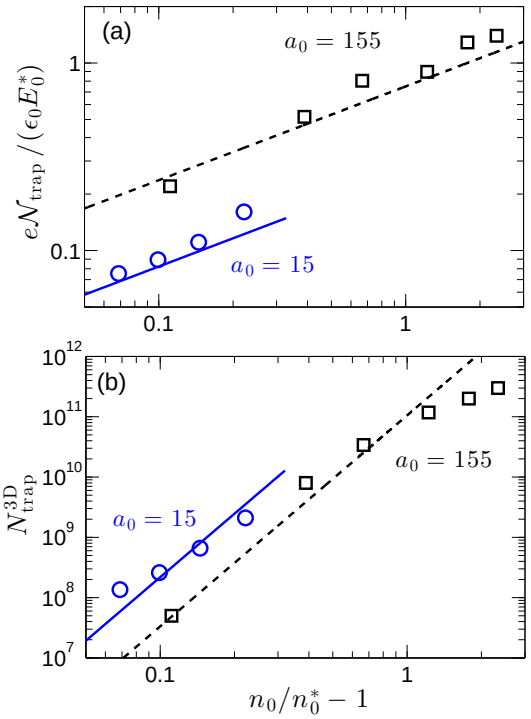

FIG. 2: (a) The number of trapped ions per area $\mathcal{N}_{\rm trap}$ and (b) the total number of the accelerated ions $N_{\rm trap}^{\rm 3D}$ for fixed laser amplitude a_0 versus $(n_0/n_0^* - 1)$, where n_0 denotes the initial target density and n_0^* the threshold density required for ion trapping. Circles and squares refer to 3D PIC simulations and the lines in (a) to Eq. (27) and in (b) to Eq. (28); blue circles (case 1, $a_0 = 15$, $n_0^* = 6.5 n_c$) correspond to the laser parameters used in Fig. (1) and black sqares (case 2, $a_0 = 155$, $n_0^* = 1.8 n_c$) to simulations reported in Ref. [7].